



**In-situ preparation of N-ZnO/graphene nanocomposites:  
Excellent impersonator as a photocatalyst for enhanced  
solar hydrogen generation and high performance  
supercapacitor electrode**

Journal:	<i>Journal of Materials Chemistry A</i>
Manuscript ID:	TA-ART-06-2015-003955.R1
Article Type:	Paper
Date Submitted by the Author:	26-Jun-2015
Complete List of Authors:	Bhirud, Ashwini; Centre for Materials for Electronic Technology, sathaye, shivaram; 758/83 Deccan Gymkhana 411004, Waichal, Rupali; National Chemical Laboratory, Park, Chan-Jin; Chonnam National University, Department of Materials Science and Engineering Kale, Bharat; Center for Material for Electronics Technology, ; C-MET,



Journal Name

ARTICLE

## In-situ preparation of N-ZnO/graphene nanocomposites: Excellent impersonator as a photocatalyst for enhanced solar hydrogen generation and high performance supercapacitor electrode

Received 00th January 20xx,  
Accepted 00th January 20xx

DOI: 10.1039/x0xx00000x

www.rsc.org/

Ashwini Bhirud<sup>a</sup>, ShivaramSathaye<sup>b</sup>, RupaliWaichal<sup>c</sup>, Chan -Jin Park<sup>d,\*</sup>, Bharat Kale<sup>a,d,\*</sup>

We have demonstrated a facile, in-situ wet chemical method to synthesize nanostructured nitrogen doped ZnO /Graphene (N-ZnO/GR) nanocomposites for the first time. Nitrogen doped ZnO over graphene (N-ZnO/GR) was studied using various concentration of graphene. During the synthesis of N-ZnO/GR nanocomposites, in-situ formation of graphene via GO reduction and formation of 4-9 nm N-ZnO have been demonstrated. The composite N-ZnO/GR absorbs in visible region and this property is used for the photocatalytic reaction to transform hazardous H<sub>2</sub>S waste into eco-friendly hydrogen using solar light. The N-ZnO/GR nanocomposite with 0.3% graphene exhibits enhanced photocatalytic stable hydrogen production rate i.e. ~5072 μmole h<sup>-1</sup> under visible light irradiation. It is noteworthy that the N-ZnO/GR electrode exhibits high specific capacitance of 555 F g<sup>-1</sup> and excellent cyclic performance with nearly 96.20 % capacity retention after 2000 cycles at current density of 10 A g<sup>-1</sup>. These results indicate great potential application of N-ZnO/GR in developing high hydrogen production and supercapacitor with high energy and power densities.

### 1. Introduction

Graphene is a rising star on the horizon of materials science and condensed matter physics.<sup>1</sup> Graphene, a two-dimensional sp<sup>2</sup> carbon network, has attracted a lot of attention due to its outstanding mechanical, thermal, optical and electrical properties, since its discovery in 2004.<sup>2</sup> Especially, it possesses a high thermal conductivity (~5000 W m<sup>-1</sup> K<sup>-1</sup>), ensures an excellent mobility of charge carriers (200 000 cm<sup>2</sup> V<sup>-1</sup> s<sup>-1</sup>) and exhibits an extremely high

theoretical specific surface area (~2600 m<sup>2</sup> g<sup>-1</sup>).<sup>3</sup> Moreover, functional graphene can be prepared through the low-cost solution-based processes, which offer tremendous opportunities for the synthesis of functionalized graphene-based composite materials.<sup>4</sup> Recently, it has been shown that the composite formed by decorating functional graphene with semiconductor materials can be used in various fields, including sensors,<sup>5</sup> electrochemical capacitors/ supercapacitors,<sup>6</sup> lithium ion batteries (LIBs),<sup>7</sup> photocatalysts<sup>8</sup> etc.

Hasty industrialization is alarming due to various environmental problems where air pollution is an important concern, globally. Among these problems, air pollution is an important concern for humans. H<sub>2</sub>S is one of the main by-product (industrial products) in coal and petroleum industries, natural gas, oil wells and geothermal plants<sup>9</sup> causing air pollution. Scarcity of energy is another important problem of modern day living due to dwindling oil/coal deposits. Therefore, dealing these two problems is at the top in the work priorities of scientists and technologists. Thus, concomitant hydrogen production and H<sub>2</sub>S decomposition are highly desirable as energy and pollution concerned ecofriendly process. In this context, photocatalytic H<sub>2</sub>S splitting under visible light has great significance

<sup>a</sup>Centre for Materials for Electronic Technology, Panchawati, Off Pashan Road, Pune 411008, India. E-mail: \*kbb1@yahoo.com

<sup>b</sup>759/83 Deccan Gymkhana, Pune 411004, India.

<sup>c</sup>National Chemical Laboratory (NCL), Dr.HomiBhabha Road, Pune-411008, India.<sup>d</sup>Department of Materials Science and Engineering, Chonnam National University 77, Yongbongro, Bukgu, Gwangju, Korea.

E-mail: \*parkcj@jnu.ac.kr

†Electronic Supplementary Information (ESI) available: Raman of GO, XPS of GO, FTIR of samples GO, Z1, Z3, Z4, Z5 and Z6, FESEM of GO, undoped ZnO and N-ZnO, TEM of Z3, hydrogen evolution of recycled Z4 sample, XRD of sample (Z4) after three cycles of photocatalytic study, Raman spectrum of sample Z4 after three cycles of photocatalytic study, XPS of sample (Z4) after three cycles of photocatalytic study. See DOI: 10.1039/x0xx00000x

as it helps to curtail the air pollution as well as economical and ecofriendly energy alternative using abundant sunlight.

Metal oxide nanomaterials are presenting themselves as one of the most important class of materials due to their excellent properties and wide applications in various fields.<sup>10</sup> Among various metal oxide nanomaterials, zinc oxide (ZnO) is one of the smart materials due to their high chemical stability, non-toxicity, high oxidation capacity, abundant availability, high specific energy density and eco-friendliness.<sup>11</sup> The band gap of ZnO is 3.2 eV, which is not effective for visible light driven photocatalysis. Therefore, using pure ZnO, efficient solar energy conversion would be unreasonable. Hence, in view of using visible part of the solar spectrum, many researchers have tried to dope ZnO with transition metals and investigated photocatalytic activity. However, they have also discussed the drawbacks of such doping<sup>12</sup> consequently, anionic doping such as N, C, and S in ZnO received great attention. The anionic doping tunes the band gap of ZnO well within the visible region, enhancing the absorption of visible light and consequently, production of maximum charge carriers. Additionally, significant overlapping of 'p' orbitals of anionic dopants with that of valence band O2p orbitals, resulting in lowering the recombination of charge carriers (electron-holes) and enhancing the photocatalytic activity.<sup>13</sup> Therefore, the researchers are still attempting to synthesize effective ZnO based photocatalysts by this route and hoping to enhance quantum yield by lowering the recombination of electron-hole pairs.<sup>14</sup> However, many researchers have tried TiO<sub>2</sub>/GR composites without doping.

Owing to the high specific surface area and superior electron mobility of graphene, it is considered to be a high performance support for photocatalysts and photocatalysis. As a result, it encouraged researchers to synthesize the N-ZnO/GR composites to maximize photocatalytic activity by exploiting efficient utilization of charge-carriers availed from doping and large number of active centers arising due to ZnO NPs deposited on high surface area of graphene sheets. Also, the same composition could be explored for its potential applications such as supercapacitors.

Recently, supercapacitors have attracted significant attention as energy-storage devices due to their high power density, rapid charge-discharge ability, low maintenance cost and long cycle life.<sup>15</sup> Such storage devices can find applications in hybrid electric vehicles, mobile electronic devices, and memory backup systems.<sup>16</sup> Furthermore, supercapacitors have less detrimental effect on

environment and are safer to handle than batteries.<sup>17</sup> The specific capacitance of supercapacitors basically depends on electrode material, thus the role of electrode materials is extremely important. In the reported literature, there have been arrays of electrode materials for supercapacitor application, among those, carbon materials are most commonly used as electrode material due to their high conductivity, large surface area and stable physicochemical properties.<sup>18</sup> However, their performance is not satisfactory due to their inherent low specific energy storage capacity. Moreover, the inert surface of carbon materials makes it difficult for electrolyte to further penetrate into the internal layers of carbon. However, to make use of advantageous properties of carbon base materials and to overcome inherent problems, mentioned above, different techniques have been used such as fabrication of composites by introducing metal oxides/ hetero atoms/oxygen in carbon materials. A suitable choice of metal oxide/chalcogenide and forming composites with graphene seem to be a better way to address these issues.<sup>19</sup>

Recently, we have demonstrated the anionic doping in TiO<sub>2</sub> and its graphene composite has been reported earlier by us.<sup>20</sup> However, many researchers have tried TiO<sub>2</sub>/GR composites without doping.<sup>21</sup> ZnO/GR composites are reported to enhance the photocatalytic activity and supercapacitive performance over their individual components namely ZnO and graphene. Xiaochen Dong and peng chen<sup>22</sup> have synthesized graphene/ZnO hybrid electrodes by an in-situ growth of ZnO nanorods on CVD grown graphene foams to form supercapacitor (~400 F g<sup>-1</sup>) having an excellent cycle life. Yi-Jun Xu<sup>23</sup> synthesized reduced graphene oxide/ZnO (RGO/ZnO) by facile solvothermal method for photocatalytic degradation of methylene blue and reduction of Cr (VI). D. Bahadur<sup>24</sup> synthesized ZnO-RGO nanohybrids by solvothermal method and showed to achieve a specific capacitance as 107.0 F g<sup>-1</sup>. Yan Feng<sup>25</sup> prepared ZnO-reduced graphene oxide by an in-situ gelatin-assisted hydrothermal synthesis for photocatalytic degradation of methylene blue. Yi-Jun Xu<sup>26</sup> synthesized ZnO nanosphere/graphene composite, ZnO nanorods/graphene composite and ZnO crystal/ graphene composites for the photocatalytic degradation of Rhodamine B, methylene blue and reduction of Cr(VI), respectively.

Authors have already reported a simple wet chemical method for the synthesis of N-ZnO nanoparticles and their application for photocatalytic H<sub>2</sub> production through H<sub>2</sub>S splitting.<sup>27</sup> In view of further improvement in this development, we have synthesized in-

situ N-ZnO nanoparticles deposited onto the surface of multi-layers graphene sheets, well known for having large surface area. Photocatalytic properties of the as-obtained product were investigated for H<sub>2</sub> production through H<sub>2</sub>S splitting. The results show that the prepared N-ZnO/GR nanocomposites possessed higher photocatalytic activity and wider response in the visible region than undoped ZnO, N-ZnO and ZnO/GR composite.

Although, the phenomena of photocatalysis and electrochemical energy storage have no direct correlation, many characteristic properties of the materials are common. For example, both prefer high surface area materials, the component interface in the composite facilitate charge transfer, ease of access to the active sites for the substrates/photons/electrolyte ion etc. After the characterization of samples for photocatalytic process, it occurred to us that many of the requirements for the application of energy storage are quite similar. We therefore decided to test these samples for energy storage applications as well. Moreover, N-ZnO/GR composite has not been attempted for energy storage application so far. Thus, in the present communication, N-ZnO/GR composite has been demonstrated for supercapacitor application with an enhanced specific capacitance of 555 F g<sup>-1</sup> at the current density of 10 A g<sup>-1</sup>. It also showed acceptable high rate capability and good cycling stability. The strategy of using a composite material synthesized from N-ZnO nanoparticles and carbon based materials as multifunctional active materials for both photocatalysis and supercapacitor has not been reported hitherto.

## 2. Experimental part

### 2.1 Preparation of Graphene oxide (GO)

Graphene oxide was prepared from graphite powder (99.99% S d fine) by a Hummers and Offeman method.<sup>28</sup> The detailed preparation method is given in ESI.†

### 2.2 Preparation of Nitrogen doped ZnO/graphene (N-ZnO/GR)

N-ZnO/Gr was prepared by using a simple wet chemical method. Analytical grade Zinc chloride (ZnCl<sub>2</sub>), urea and absolute ethanol were purchased from the local chemical manufacturer (Qualigene chemicals) and used as received. In a typical synthesis, the as prepared GO, (0.3%, 0.6% and 0.8%,) was dispersed in absolute ethanol and ultrasonicated for half an hour [Solution A]. To a solution of 0.5 M ZnCl<sub>2</sub> in absolute ethanol, urea (1:2 w/w of ZnCl<sub>2</sub>:urea) was added slowly with constant stirring until a

homogeneous solution was achieved [solution B]. Then, solution 'B' was slowly added into solution 'A' with constant stirring. The stirring was continued for additional half an hour. This final solution was then kept in oven at 150°C to obtain a black product i.e a mixture of Zn-urea-graphene intermediate complex and excess biurea, which was found to be hygroscopic. The hygroscopic product was preserved in a desiccator and then further subdivided for heat treatment in air at 500°C, 600°C, 700°C and 800°C for 3h to obtain the desired product i.e. N-doped ZnO/GR, which was no longer hygroscopic. Simultaneously, undoped ZnO, N-doped ZnO and ZnO/GR were prepared for comparison, following the similar procedure. Chronologically, the products annealed at 500°C are labelled as Z1, Z2. The sample was prepared by heat treating 0.5 M ZnCl<sub>2</sub> and as prepared GO (with 0.3% loading) in absolute ethanol (without any additives like urea) at 150°C to obtain an intermediate product which was further annealed at 500°C for 3h and denoted as Z3. The other products with dopants and graphene composites with 0.3%, 0.6% and 0.8% (w/w) loading of GO were annealed at 500°C for 3h and denoted as Z4, Z5 and Z6 respectively. After annealing, all the samples were washed with copious amounts of hot distilled water until all chlorine is removed and these products were then subjected to XRD, DRS, Raman, XPS, FTIR, FESEM, HRTEM, BET and PL analysis for their characterization.

### 2.3 Characterization

The optical properties of the powder samples were studied using an UV-visible-near infrared spectrometer (UV-VIS-NIR, Perkin Elmer Lambda-950). The crystalline phases and the crystallite size of the photocatalyst was identified using an X-ray powder diffraction (XRD) technique (XRD-D8, Advance, Bruker-AXS) with Cu K $\alpha$  radiation. Room temperature micro Raman scattering (RS) was performed using a HR 800-Raman Spectroscopy, Horiba Jobin Yvon, France, with an excitation at 632.81 nm by a coherent He-Ne ion laser and a liquid nitrogen cooled CCD camera to collect and process the scattered data. The nature of chemical bonds formed in N-ZnO and reduction of GO to graphene were examined using X-ray photoelectron spectroscopy (XPS, ESCA-3000, VG Scientific Ltd, England) with a base pressure greater than 1.0  $\times$  10<sup>-9</sup> Pa and Mg K $\alpha$  radiation (1253.6 eV) was used as an X-ray source operated at 150 W. FTIR spectra were recorded with a Nicolet Magna 550 spectrometer. The morphologies of the N-ZnO/GR composites nanostructures were characterized by field emission scanning electron microscopy (FESEM, Hitachi, S-4800) and high resolution

transmission electron microscopy (HRTEM, JEOL, 2010F). For HRTEM studies, samples were prepared by dispersing the powder in acetone, followed by sonication in an ultrasonic bath for 2 min and then drop-casting the dispersion on a carbon coated copper grid and by subsequent drying in a vacuum. The Brunauer-Emmett-Teller (BET) specific surface area ( $S_{\text{BET}}$ ) of the powders was analyzed by nitrogen adsorption in a Micromeritics ASAP 2020 nitrogen adsorption apparatus (U.S.). All of the prepared samples were degassed at 180°C prior to nitrogen adsorption measurements. Photoluminescence (PL) emission spectra were recorded using HORIBA-JY, F-3 Fluorescence spectrophotometer, excited at 300 nm.

#### 2.4 Photodecomposition of H<sub>2</sub>S

The cylindrical quartz photochemical reactor was filled with 200 ml 0.25 M aqueous KOH and purged with argon for 1 h. Hydrogen sulphide (H<sub>2</sub>S) was bubbled through the solution (KOH) for about 1 h at the rate of 2.5 ml min<sup>-1</sup> at 299 K. 0.2 gm of each photocatalyst namely, undoped ZnO, N-ZnO, ZnO/GR and N-ZnO/GR respectively, was introduced once at a time into the reactor and irradiated with a visible light source Xe-lamp (300 W, LOT ORIEL GRUPPE, EUROPA, LSH302) and stir constantly. The escaped hydrogen sulfide was trapped in a NaOH solution. The amount of hydrogen gas evolved was collected in a graduated cylinder and measured. The evolved hydrogen was then analyzed for its purity using a gas chromatograph (Model Shimadzu GC-14B, MS-5 Å column, TCD, Ar carrier). All the samples (Z1–Z6) were tested for their catalytic activity under identical conditions.

#### 2.5 Electrochemical measurements

The electrochemical measurements were carried out in a three electrode electrochemical cell containing 1 M Na<sub>2</sub>SO<sub>4</sub> as the electrolyte. In the three electrode CV system, the undoped ZnO (Z1), N-ZnO (Z2), ZnO/GR (Z3) and N-ZnO/GR (Z4) composite serves as the working electrode, an Ag/AgCl electrode as the reference, and a platinum wire as the counter electrode. The working electrode was prepared by mixing N-ZnO/GR and polyvinyl difluoride (PVDF) in ethanol, pasted on to nickel foam (~1 cm<sup>2</sup>) and then dried at 60°C for 12h. The loaded mass of each electrode was about 63mg (undoped ZnO, Z1), 64mg (N-ZnO, Z2), 63mg (ZnO/GR, Z3) and 65mg (N-ZnO/GR, Z4), respectively. Cyclic voltammetry (CV) and galvanostatic charge–discharge were performed by an Autolab PGSTAT 30 (Ecochemie) electrochemical workstation at room temperature. CVs were taken between -0.5 to 0.5 V at

different scan rates. Galvanostatic charge–discharge measurements were measured in the potential range of 0 to 1.0 V at different current densities. Electrochemical impedance spectroscopy (EIS) was carried out in the frequency range from 2 Hz to 100 kHz with an alternating current (AC) potential amplitude of 10 mV.

### 3. Results and discussion

To understand the formation mechanism of the final product N-ZnO/GR, we refer to the formation of N-ZnO which is discussed in our previous publication.<sup>27</sup> The formation of N-ZnO/GR does not change the mechanism of formation either qualitatively or quantitatively by the small amount of GO addition.

The phase purity of ZnO in samples is confirmed by the XRD. Fig. 1 shows the XRD pattern for undoped ZnO (Z1), N-ZnO (Z2), ZnO/GR(Z3) and N-ZnO/GR nanocomposites (Z4–Z6) synthesized with different percent of graphene.

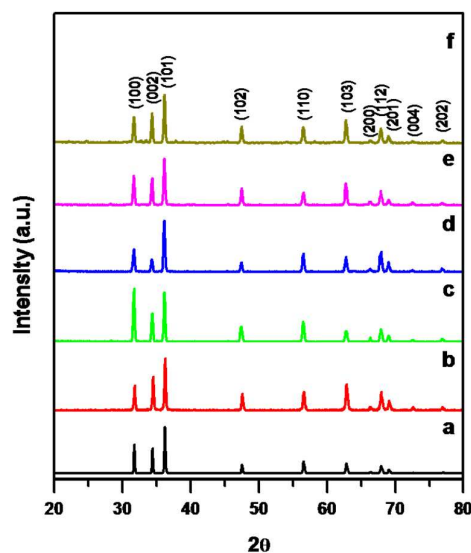


**Fig. 1** XRD spectrum of samples (a) undoped ZnO (Z1) treated at 800°C for 3h (b) N-ZnO treated at 500°C for 3h (Z2) (c) ZnO/GR nanocomposite with 0.3% loading which treated at 500°C for 3h (Z3) and N-ZnO/GR nanocomposites treated at 500°C for 3h with different GO loading (d) 0.3% (Z4), (e) 0.6% (Z5) and (f) 0.8% (Z6).

The dominant peaks located at ca. 31.7, 34.4, 36.3, 47.6, 56.6, 62.9, 66.4, 68.0, 69.1, 72.6, and 77.0° are indexed to (100), (002), (101), (102), (110), (103), (200), (112), (201), (004) and (202) crystallographic planes of hexagonal ZnO (JCPDS file no. 36-1451).<sup>29</sup> The diffraction peaks for graphene are not observed in the nanocomposites of ZnO/GR and N-ZnO/GR, which may be due to small amount of graphene.<sup>30</sup>

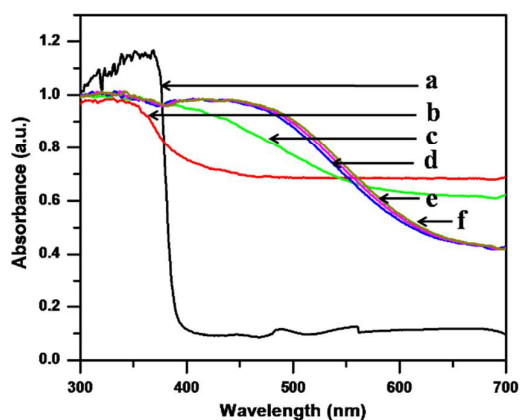


**Fig. 2** UV-DRS spectra of samples (a) undoped ZnO (Z1) treated at 800°C for 3h (b) N-ZnO treated at 500°C for 3h (Z2) (c) ZnO/GR nanocomposite with 0.3% loading which treated at 500°C for 3h (Z3) and N-ZnO/GR nanocomposites treated at 500°C for 3h with different GO loading (d) 0.3% (Z4), (e) 0.6% (Z5) and (f) 0.8% (Z6).

Fig. 2 shows the UV-vis diffuse reflectance spectra of undoped ZnO (Z1), N-ZnO (Z2), ZnO/GR (Z3) and N-ZnO/GR (Z4-Z6) nanocomposites. The spectrum shows the absorption edge at 388 nm (3.19 eV) for undoped ZnO powder, as is commonly observed for wurtzite ZnO. N doping significantly shifts the absorption edge to the visible region as observed in spectra in Fig. 2. Further observation demonstrates that the absorbance in visible light region increases due to the co-operative effect of nitrogen doping and graphene. The optical absorption shows a red-shift with the incorporation of 'N' dopant.<sup>31</sup> It is obvious that N-ZnO/GR shows much higher visible light absorption than ZnO/GR composite. When 'N' were introduced into ZnO/GR composite, the absorption of nitrogen and graphene modified ZnO is extended to 652 nm. Therefore, the results obviously demonstrate the significant influence of graphene and 'N' doping on the optical properties; suggesting incorporation of graphene and 'N' anion enhance the visible-light absorption and is expected to improve the visible-light photocatalytic activity.<sup>30</sup>

Raman spectroscopy is widely employed to study the ordered/disordered crystal structures of carbonaceous materials.

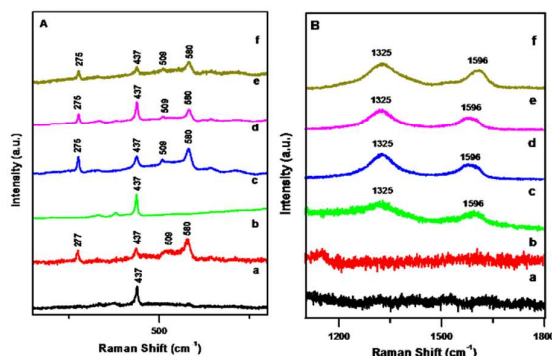


**Fig. 3**(A, B) Raman spectrum of samples (a) undoped ZnO (Z1) treated at 800°C for 3h (b) N-ZnO treated at 500°C for 3h (Z2) (c) ZnO/GR nanocomposite with 0.3% loading which treated at 500°C for 3h (Z3) and N-ZnO/GR nanocomposites treated at 500°C for 3h with different GO loading (d) 0.3% (Z4), (e) 0.6% (Z5) and (f) 0.8% (Z6). (B) shows the magnified area from 1100-1800  $\text{cm}^{-1}$ .

Fig. 3A shows a comparison of the Raman spectra of undoped ZnO (Z1), N-ZnO (Z2), ZnO/GR (Z3) and N-ZnO/GR (Z4-Z6) samples. In case of GO (Fig. S1), there are two typical Raman bands located at 1325 and 1596  $\text{cm}^{-1}$ , which correspond to disordered  $\text{sp}^2$  carbon (D-band) and well-ordered graphite (G-band), respectively.<sup>32</sup> In all the spectra, a common Raman line is located at 437  $\text{cm}^{-1}$  (Fig. 3(A) a-f), which corresponds to the E2 (high) vibrational mode of wurtzite structure. The signals at A1 (275–277  $\text{cm}^{-1}$ ), A3 (509  $\text{cm}^{-1}$ ) and A1 (LO) (580  $\text{cm}^{-1}$ ) can be assigned to local vibration modes (LVMS) of nitrogen in ZnO.<sup>33</sup> Raman mode at 275  $\text{cm}^{-1}$  was attributed to the localized vibration of Zn atoms, where parts of their first nearest neighbour O atoms are replaced by N atoms in the ZnO lattice.<sup>34</sup> Further, the Raman peaks observed at 509 and 580  $\text{cm}^{-1}$  are related to the presence of nitrogen in ZnO structure.<sup>35</sup> The Raman spectroscopic observations, thus confirms N-doping in the ZnO lattice.<sup>24</sup> Additionally, in chemically processed samples of Z3-Z6, Raman spectra show the presence of D and G bands of graphene. For acquiring data of D and G bands in Raman spectra of samples Z3-Z6, the samples Z3-Z6 were dissolved in Con.  $\text{HNO}_3$ .<sup>36</sup> We observed that the ZnO or N-ZnO component of the composite, completely dissolved and black powder remained as a residue, presumed to be that of graphene component of the composite. The residual black powder was washed, dried and characterized by Raman spectroscopy. The Raman spectra (Fig. 3B) showed the presence of D (1325  $\text{cm}^{-1}$ ) and G (1596  $\text{cm}^{-1}$ ) bands of graphene, indicating successful incorporation of graphene in ZnO/GR composite (Z3) and N-ZnO/GR composite (Z4-Z6) respectively. Figure 3B shows the Raman spectrum of the ZnO/GR (Z3) and N-ZnO/GR (Z4-Z6)

nanocomposites exclusively in the range of 1100-1800  $\text{cm}^{-1}$ . It is quite clear that those two prominent peaks centred at about 1325  $\text{cm}^{-1}$  (D band) and 1596  $\text{cm}^{-1}$  (G band) suggesting that the structure of graphene is retained in the composite.

2D peak of Raman spectrum, observed at  $\sim 2700 \text{ cm}^{-1}$ , is a reliable test to confirm the presence of a monolayer or few layer graphene.<sup>37</sup> However, with increasing number of layers of graphene, 2D peak becomes broader and less intense and disappear beyond 5-6 layers of graphene. In these cases, it is reported that increased D/G intensity ratio as compared to that of GO is an indicator of the presence of graphene.<sup>38</sup>

In general, the D/G intensity ratio is a measure of disorder degree and average size of the  $\text{sp}^2$  domains in graphite materials.<sup>39</sup> Hence, a higher D/G peak intensity ratio indicates more defects and disorders of the graphitized structures mostly, at the edges of the carbon sheets. Compared with GO (ID/IG = 0.93), the increased D/G intensity ratios are observed for samples Z3 (1.13), Z4 (1.47), Z5 (1.36), Z6 (1.30) respectively. This implies that GO has been reduced to graphene with dominant  $\text{SP}^2$  hybridized structure with large number of defects.

XPS was used to provide further evidence for the nitrogen doping in ZnO lattice, reduction of GO and the chemical composition of N-ZnO/GR (Z4) nanocomposite.

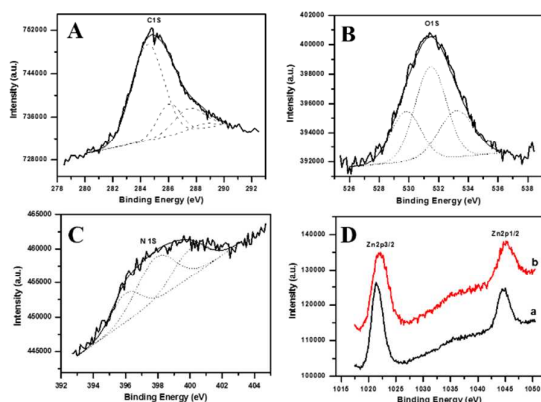


**Fig. 4** XPS patterns of N-ZnO/GR nanocomposite with 0.3% GO loading synthesized at 500°C for 3h (Z4) (A) C1s, (B) O1s, (C) N1s, (D) Zn 2p of (a) undoped ZnO (Z1) and (b) N-ZnO/GR (Z4).

Fig. 4 shows the high resolution XPS spectra for C1s, N1s, O1s and Zn2p core levels of the N-ZnO/GR composite. The XPS spectrum of C 1s in GO (Fig. S2) is deconvoluted into three main components. The peak at 284.6 eV is attributed to  $\text{sp}^2$  carbon atom (C-C, C=C and C-H groups), while the peak centered at 286.7 eV is assigned to the C

from the C-OH and C=O groups.<sup>40</sup> The peak located at 288.5 eV is closely associated with the O=C-OH species.<sup>41</sup> Compared with the C1s spectrum of GO, the intensity of peaks due to C-OH, C=O and O=C-OH in C1s spectrum of N-ZnO/GR (Z4) prominently decreased, implying the substantial reduction of GO during the composite formation (Fig. 4A). Meanwhile, a new peak at 287.6 eV can be observed, which is attributed to the Zn-O-C bond.<sup>42</sup> These results indicated the successful stabilized/anchored deposition of ZnO on the graphene surfaces and also lowering of the oxygenated functional groups. Fig. 4B shows the high resolution XPS spectra of O1s after deconvolution wherein oxygen exists at least in three forms with binding energies 529.8, 531.5, 533.3 eV, respectively. The peak at 529.8 eV is mainly assigned to the oxygen atoms coordinated with Zn atoms.<sup>43</sup> The peak at 531.5 eV corresponds to oxygen adsorbed on sample surface probably as (-OH).<sup>44</sup> The peak at 533.3 eV is likely to be due to water molecules on the surface.<sup>45</sup> Fig. 4C show that N1s peaks appeared at 396.0, 397.9, 400.0 eV which indicate nitrogen incorporation. These three peaks are assigned to N-Zn, N-C and N-H bonds respectively.<sup>46</sup> Fig. 4D shows the XPS spectra of Zn (2p) for undoped ZnO and N-ZnO/GR (Z4) composite. The peaks at 1021.4 eV and 1044.6 eV in undoped ZnO correspond to the Zn (2p) doublets 2p<sub>3/2</sub> and 2p<sub>1/2</sub> which is associated with the  $\text{Zn}^{2+}$  in ZnO wurtzite structure. There is a slight shift to higher binding energy in Zn(2p) spectrum of N-ZnO/GR (Z4) that indicates a change in chemical binding of Zn.<sup>42</sup> Additionally, the average O/C atomic ratio of N-ZnO/GR (Z4) sample is 0.17 which is much smaller than 0.35 for pure GO. The decrease of O/C atomic ratio further confirms the partial reduction of GO. The presence of small amount of hydrophilic groups on the surface of graphene, such as hydroxyl and carboxyl, can be helpful to enhance the photocatalytic activity.<sup>47</sup>

FTIR spectra of GO, undoped ZnO (Z1), N-ZnO (Z2), ZnO/Gr (Z3) and N-ZnO/GR(Z4-Z6) nanocomposites are shown in Fig. S3 (A, B). For GO, the peaks at 962, 1059, 1250, 1560 and 1725  $\text{cm}^{-1}$  are assigned to the epoxy stretching, alkoxy C-O stretching, C-O-C stretching, vibrations of aromatic C=C  $\text{sp}^2$  hybridized carbons and C=O stretching vibration respectively.<sup>48,49</sup> After the reaction of composite formation, FTIR of N-ZnO/GR (Z4-Z6) nanocomposite shows no signatures of peaks due to C-O stretching, C=C  $\text{sp}^2$  hybridized carbon and C=O stretching. Also, apart from these observations, peaks at 962  $\text{cm}^{-1}$  and 1250  $\text{cm}^{-1}$  are observed which can be assigned to epoxy stretching and C-O-C stretching functional

groups. The absorption band at  $480\text{ cm}^{-1}$  in undoped ZnO (Z1) is assigned to the stretching vibration of Zn-O. The ZnO/GR(Z3) and N-ZnO/GR (Z4-Z6) nanocomposites show a broad band in the range  $450\text{--}650\text{ cm}^{-1}$ . All these changes considered together, suggest that during the composite formation, GO gets partially reduced to graphene which is attached to surrounding ZnO species; wherein 'O' acts as a bridging atom. This proposal is consistent with XPS studies where Zn-O-C bond formation is indicated.

Fig. 5 shows the morphology of the as-obtained samples. GO, undoped ZnO(Z1), N- ZnO (Z2), ZnO/GR (Z3) and N-ZnO/GR (Z4-Z6) samples were investigated by field emission scanning electron microscopy (FESEM) and high resolution transmission electron microscopy (HRTEM).

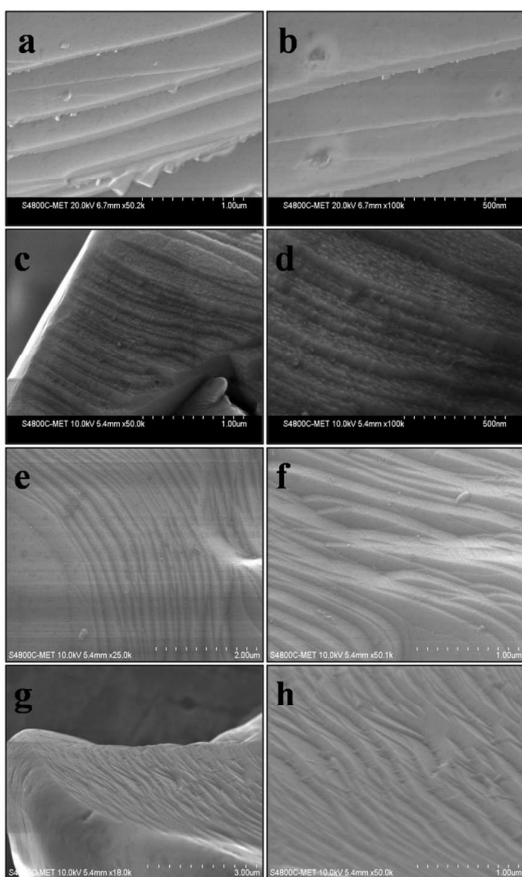


**Fig. 5** FESEM of samples (a, b) ZnO/GR nanocomposite with 0.3% loading which treated at  $500^{\circ}\text{C}$  for 3h (Z3) and N-ZnO/GR nanocomposites treated at  $500^{\circ}\text{C}$  for 3h with different GO loading (c, d) 0.3% (Z4), (e, f) 0.6% (Z5) and (g, h) 0.8% (Z6).

Fig. S4 (a, b) shows the FESEM image of GO in which most of the nanosheets are curled and stacked together with a layered structure. FESEM of undoped ZnO (Z1) (see supplement materials

Fig. S4 c, d) shows the agglomerated hexagons of sizes  $\sim 3\text{--}6\text{ }\mu\text{m}$ . Fig. S4 (e, f) shows N-ZnO with spongy structure. FESEM of ZnO/GR (Z3) sample (Fig. 5 a, b) shows the ZnO nanoparticles deposited on graphene sheets and the size of nanoparticles is in the range of  $4\text{--}9\text{ nm}$  (Fig. S5: TEM images). Fig. 5 (c–h) shows the FESEM images of N-ZnO/GR composites with small N-ZnO nanoparticles are anchored on the surface of graphene sheets. Such an anchoring can be imagined to occur through the interaction between 'O' from GO and the defect sites of graphene, especially at edges and the species derived from Zn precursor. Graphene layers stack with each other through the van der Waal interactions to form an open system, through which electrolyte ions easily access the surfaces of graphene. This facilitates the reversible electrolyte ion movement in and out of graphene layers separated by ZnO particles and improve the electrochemical utilization of ZnO or N-ZnO.

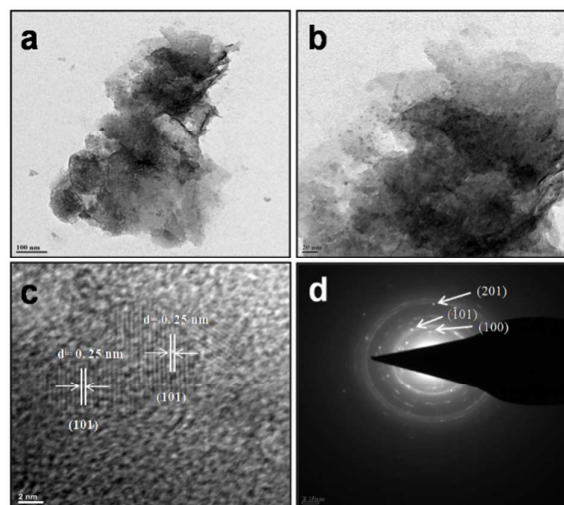
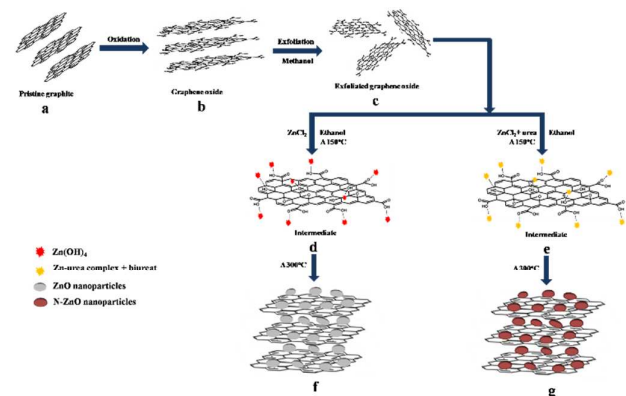


**Fig. 6** TEM of N-ZnO/GR nanocomposite with 0.3% GO loading which treated at  $500^{\circ}\text{C}$  for 3h (Z4).

We have also characterized the N-ZnO/GR(Z4) sample by HRTEM (Fig. 6 a–d). In the TEM images (Fig. 6 a, b) we observed  $\sim 5\text{ nm}$  sized nanoparticles on the graphene sheet. The HRTEM image (Fig. 6 c) of individual N-ZnO nanoparticles showing clear lattice fringes with spacing of ca.  $0.25\text{ nm}$  which corresponds to (101) lattice planes of the ZnO. The selected area electron diffraction (SAED) pattern (Fig. 6 d) indicates that the composite consists of crystalline phases. The electron diffraction dots can be indexed as the (100), (101) and (201) planes of the hexagonal wurtzite phase of un-agglomerated ZnO nanoparticles. These observations are consistent with the XRD results (Figure 1).

The formation mechanism of ZnO/GR and N-ZnO/GR nanocomposite is illustrated in scheme 1.



**Scheme 1** Schematic representation of formation mechanism of ZnO/GR and N-ZnO/GR nanocomposites.

GO, prepared by the Hummer's method via pristine graphite (scheme 1b) and zinc chloride were mixed in an absolute ethanol for the synthesis of ZnO/GR composite (Z3). For the N-ZnO/GR composites (Z4-Z6), the GO prepared using the Hummer's method and zinc chloride along with urea were mixed in an absolute ethanol. During ultrasonic pre-treatment, (scheme 1c) van der Waals interactions among the GO layers are overpowered leading to the separation of GO sheets. Concomitantly, zinc chloride and urea which are present in the same solvent interact to form Zn-urea complex/ $\text{Zn}(\text{OH})_2$ . These products subsequently interact with oxygen containing species of GO, resulting in the formation of Zn-urea-GO complex along with other by-products such as biuret etc.<sup>27</sup> Thus, Zn species get anchored on the graphene through oxygen site of GO, possibly through bonding (Zn-O-GR) (scheme 1d, e).<sup>50</sup> During all these interactions, the driving reaction for GO to develop graphene by reduction occur due to the reducing property of ammonia released from urea at moderately high temperatures.<sup>51</sup> Further, the complex along with biuret heated at 500 °C lead to the formation of  $\text{ZnO}_{1-x}\text{N}_x$  on the graphene.<sup>27</sup> Thus, N-ZnO nanoparticles either grow on graphene sheets or/and get attached to graphene through bond formation to form N-ZnO/GR nanocomposite (scheme 1f). In absence of urea, obviously, only formation of ZnO on graphene occurs. (Scheme 1g).

As shown by previous studies, GO sheets have their basal planes covered mostly with epoxy and hydroxyl groups, while carbonyl and carboxyl groups are located at the edges.<sup>52</sup> These functional groups, acting as anchor sites, enable the subsequent in-situ formation of nano- structures wherein semiconductor gets attached to the

surfaces and edges of GO sheets through bond formation. However, these oxygen-containing functional groups impair the conductivity of GO sheets and hence they are no longer suitable as electrode materials. On the other hand, graphene sheets have an excellent conductivity and therefore an ideal substrate for the growth of functional composite nanomaterials to render them electrochemically active. This can offer more active adsorption sites and photocatalytic reaction centers. Therefore, it is expected to offer an enhanced photocatalytic activity and electrochemical properties.

The effect of graphene on the BET surface area ( $S_{\text{BET}}$ ) of the as prepared composite samples was also investigated. N-ZnO/GR composite samples (Z4-Z6) show higher BET surface area ( $75.19\text{--}81.90\text{ m}^2\text{g}^{-1}$ ) than observed for undoped ZnO (Z1) ( $26.56\text{ m}^2\text{g}^{-1}$ ), N-ZnO (Z2) ( $45.26\text{ m}^2\text{g}^{-1}$ ) and ZnO/GR (Z3) ( $40.14\text{ m}^2\text{g}^{-1}$ ). It is clear that nitrogen doping is effective for enhancing surface area. Furthermore, graphene addition shows an improvement in specific surface area of composite, over and above that shown by nitrogen doping. Also, as shown in Table 1, the BET surface area decreases with the increase of graphene content beyond optimized 0.3%. A greater specific surface area of photocatalysts can supply more surface active sites and make charge carriers transport easier, leading to an enhancement of the photocatalytic performance.<sup>53</sup> Thus, the role of graphene in enhancing the photocatalytic activity is justified.

#### Photocatalytic study

The photocatalytic activity of the undoped ZnO (Z1), N-ZnO (Z2), ZnO/GR (Z3) and N-ZnO/GR (Z4-Z6) samples for hydrogen generation via photodecomposition of  $\text{H}_2\text{S}$  was performed.

Table 1 shows the hydrogen evolution rate from the photodecomposition of  $\text{H}_2\text{S}$  using undoped ZnO (Z1), N-ZnO (Z2), ZnO/GR (Z3) and N-ZnO/GR (Z4-Z6) under visible light. Control experiments indicated that no appreciable hydrogen production was detected in the absence of irradiation of photocatalyst, suggesting that hydrogen was produced only through photocatalytic reactions on the photocatalyst surface. The photocatalytic activity of undoped ZnO (Z1) showed a lower hydrogen evolution rate, i.e., around  $1874\text{ }\mu\text{mol h}^{-1}$ , while the N-ZnO (Z2), ZnO/GR (Z3) and N-ZnO/GR (Z4-Z6) showed 3957, 2434, 5072, 4784 and  $4267\text{ }\mu\text{mol h}^{-1}$ , respectively. The maximum  $\text{H}_2$  evolution i.e.  $5072\text{ }\mu\text{mol h}^{-1}$  was obtained for sample Z4. Thus, it can be inferred that incorporation of graphene in the composite i.e.

sample N-ZnO/GR (Z4) shows the enhanced hydrogen evolution rate which is  $\sim 1.3$  times that of N-ZnO (Z2). However, a further increase in the graphene content led to a deterioration of the catalytic performance. In particular, at the graphene content of 0.8% (Z6) sample the photocatalytic activity decreased, showing an  $H_2$ -production rate of  $4267 \mu\text{mol h}^{-1}$  as against  $5072 \mu\text{mol h}^{-1}$  shown by sample Z4. It is understandable as the introduction of a large percentage of black graphene led to shielding of the active sites on the catalyst surface and also rapidly decreased the intensity of light through the depth of the reaction solution, which has been reported as "shielding effect".<sup>54</sup> As a consequence, an optimized content of graphene is crucial for attaining the highest photocatalytic activity of N-ZnO/GR nanocomposites.

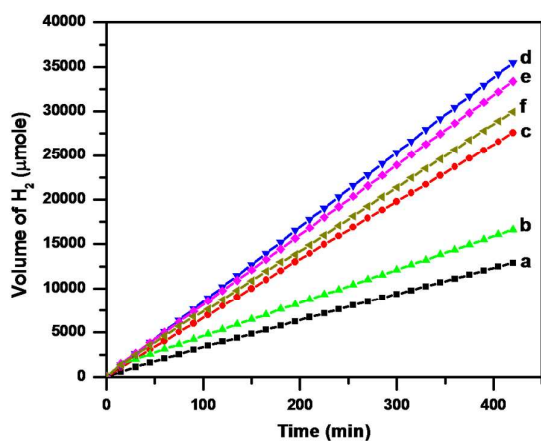
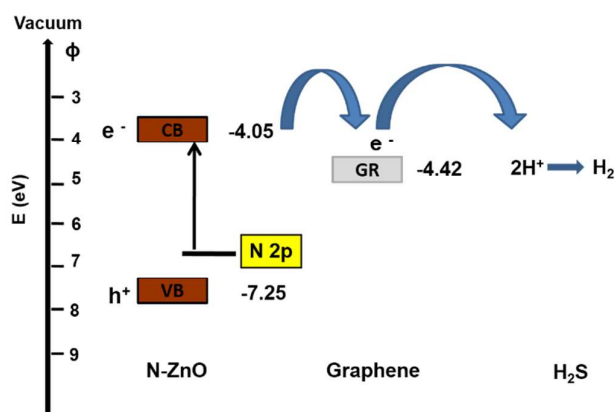


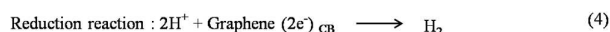
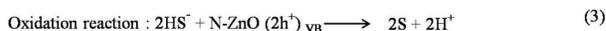
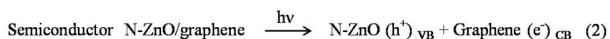
**Fig. 7** Time versus volume of  $H_2$  ( $\mu\text{mole}$ ) evolution of samples (a) undoped ZnO (Z1) treated at  $800^\circ\text{C}$  for 3h (b) N- ZnO treated at  $500^\circ\text{C}$  for 3h (Z2) (c) ZnO/GR nanocomposite with 0.3% loading which treated at  $500^\circ\text{C}$  for 3h (Z3) and N- ZnO/GR nanocomposites treated at  $500^\circ\text{C}$  for 3h with different GO loading (d) 0.3% (Z4), (e) 0.6% (Z5) and (f) 0.8% (Z6).

As seen from Fig. 7, the nitrogen doping and the graphene content has a significant influence on the photocatalytic activity of ZnO. However, overall N-ZnO/GR sample Z4 shows higher activity among the synthesized composites. In fact, presently obtained activity is more than reported for metal oxide<sup>27, 55</sup> and sulfide semiconductors studied so far.<sup>56</sup> The schematic photocatalytic reaction mechanism of N-ZnO/GR is described in scheme 2.



**Scheme 2** Schematic representation of photocatalytic mechanism of N-ZnO/GR nanocomposite

An important role of graphene in composite is as an electron acceptor as well as fast transporter to the substrate. Graphene has been reported to be competitive candidate as an acceptor material due to its  $\pi$ -conjugation structure and has excellent mobility of charge carriers and large specific surface area. Therefore, rapid transport of charge carriers could be achieved and consequent effective charge separation accomplished. Overall, both the electron accepting and transporting properties of graphene in the composite could contribute to the enhancement of photocatalytic activity.<sup>57</sup> The major reaction steps in this mechanism under visible-light irradiation are described in following equations.



The photocatalytic performance enhancement can be rationalized as creation of suitable energy levels in the band diagram of composite as shown in scheme 2. A stepwise manoeuvring of suitable composite formation for the desired reaction to occur through chemical/physical steps is as follows. 1) Pure ZnO band gap (3.2 eV) is not suitable to absorb visible portion of solar light; therefore nitrogen doping realized. The energy level of N2p impurity is above the VB of ZnO in the energy diagram. So that visible light of solar spectrum is able to excite electrons from N2p levels to conduction band. 2) Thus, excited electrons are energetically suitably transferred to graphene whose CB is below the CB of ZnO on absolute scale. Thus, the recombination of

electrons-holes is minimized. 3) Since graphene has a very good charge transport properties, resulting charge separation shown by equation (2) is efficient. Also, electrons in ZnO CB are rapidly transported to substrate via CB of graphene, to achieve desired product ( $H_2$ ). 4) As mentioned earlier, graphene has a surface area much larger than that of ZnO and N-ZnO. While forming a composite N-ZnO/GR, N-ZnO gets anchored on graphene surface through bond formation or physisorption. Thus, the large surface area of graphene causes enhanced number of active centers over ZnO and N-ZnO phases available for the reaction. Moreover, ZnO and N-ZnO particle growth gets restricted as particle get dispersed on large surface area of graphene. Since, very tiny N-ZnO nanoparticles deposited on graphene, the maximum absorption of visible light has been favoured which leads to formation of higher charge carriers. Further, easy transports of electrons due to graphene enhance the charge carrier separation. The combined effect of all these factors result in the improved  $H_2$  production.

The photoluminescence studies support this mechanism. Photoluminescence peaks' intensities are lowered by N doping as well as forming composition with graphene. The photoexcited electrons among carriers in N-ZnO/GR are transported to graphene rather than getting recombined with holes. Thus, the cause of high intensity photoluminescence of pure ZnO is affected by the creation of defect states in the band gap of ZnO and forming a composite with graphene; leading to lowering of photoluminescence intensity as shown in Fig. 8.

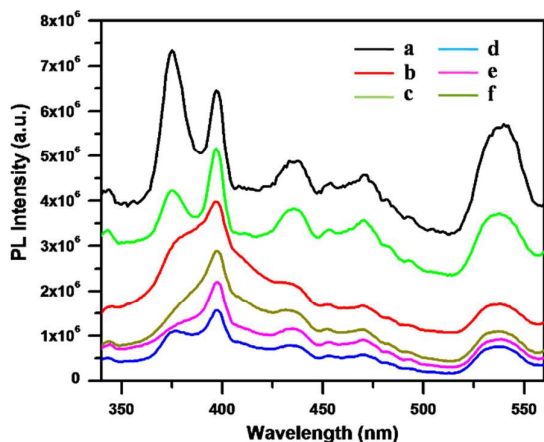


**Fig. 8** PL spectra of samples (a) undoped ZnO (Z1) treated at 800°C for 3h (b) N-ZnO treated at 500°C for 3h (Z2) (c) ZnO/GR nanocomposite with 0.3% loading which treated at 500°C for 3h (Z3) and N-ZnO/GR composites treated at 500°C for 3h with different GO loading (d) 0.3% (Z4), (e) 0.6% (Z5) and (f) 0.8% (Z6)

In PL, the two emission bands were observed in the spectra: a UV peak at around 376 nm and a broad green emission at  $\sim 536$  nm which are attributed to free excitons emission from the wide band gap of ZnO and the recombination of electrons in single occupied oxygen vacancies in ZnO nanoparticles respectively.<sup>58</sup> The photoluminescence emission occurs from the recombination of excited electrons and holes under light irradiation, the higher photoluminescence intensity shows the separation and recombination of more photo-induced electrons and holes inside the materials. If the photo-generated electrons or holes are transferred to other matters, i.e., quenched, the photoluminescence intensity will decrease. When graphene is introduced into N-ZnO, a considerable quenching was observed and the fluorescent intensity is considerably quenched as shown in Fig. 8. The reason is that the work function of graphene at  $-4.42$  eV<sup>57</sup> is favourably close for electron transfer to the N-ZnO CB energy level of  $-4.05$  eV.<sup>59</sup> Under illumination, the photogenerated electrons are injected from the CB band of N-ZnO to the CB of graphene while the holes are trapped by N-ZnO. Under such circumstances, graphene can withdraw electrons and act as electron sink. Also, graphene having 2D structure with a large specific surface area and ultrahigh electron mobility ( $>1000$  cm<sup>2</sup> V<sup>-1</sup> s<sup>-1</sup>) acts as electron-transporting bridge between N-ZnO and substrates, allows quick electron transfer to substrates, resulting in the separation of excited electron-hole pairs. This fast electron transporting process lowers the photo-generated electrons to return to the N2p level of N-ZnO or the VB level of ZnO, which will lead to a fluorescent emission. When graphene is introduced into undoped ZnO, also ensues the same effect. The fluorescence intensity is quenched in ZnO/GR (Z3) as shown in Figure 8. In the next step, the electrons derived from N-ZnO CB to graphene CB are further transported to substrate H<sup>+</sup> ions to form H<sub>2</sub>. Therefore, the synergistic effect of 1) extended visible light absorption due to 'N' doping, 2) making large number of active centers available for desired reaction to occur derived from large surface area graphene content, 3) efficient use of high charge carrier transporting properties of graphene which is in close contact with N-ZnO and 4) suitable positions of N-ZnO and graphene in energy band diagram lead to efficient charge separation and subsequent decomposition of H<sub>2</sub>S to produce H<sub>2</sub> under visible-light irradiation. To the best of our knowledge, this is the first report showing that an inexpensive N-ZnO with carbon

material can be used as an effective catalyst for photocatalytic H<sub>2</sub>S splitting.

The stability of N-ZnO/GR composite (Z4) was evaluated by performing the recycle experiments of the photocatalyst under similar experimental conditions. After three cycles of reaction, we observed almost same H<sub>2</sub> evolution (Fig. S6). This indicates noteworthy stability of the N-ZnO/GR (Z4) for hydrogen generation. The XRD, Raman and XPS of recycled catalyst (Z4) does not show any change in composition and purity of phases, implying good stability of the catalyst (Fig. S7, S8 and S9). After performing the three cycles of photocatalytic study we observed the presence of elemental 'S' and absence of 'SO<sub>4</sub>' in XPS studies (Fig. S10). In fact, these observations are in agreement with the suggested mechanism of H<sub>2</sub> generation. The formation of elemental sulphur is rather more valuable due to its application in agriculture and pharmaceutical products.

#### Electrochemical study

To evaluate the potential applications of the composites as electrochemical energy storage, the N-ZnO/GR composites were used as electrodes and characterized by cyclic voltammetry (CV) and galvanostatic charge–discharge in 1 M Na<sub>2</sub>SO<sub>4</sub> aqueous solution. Fig. 9a shows the typical CV curves of the undoped ZnO (Z1), N-ZnO (Z2), ZnO/GR (Z3) and N-ZnO/GR (Z4-Z6) electrodes with a scan rate of 200 mV s<sup>-1</sup> and a potential window of -0.5 to 0.5 V.

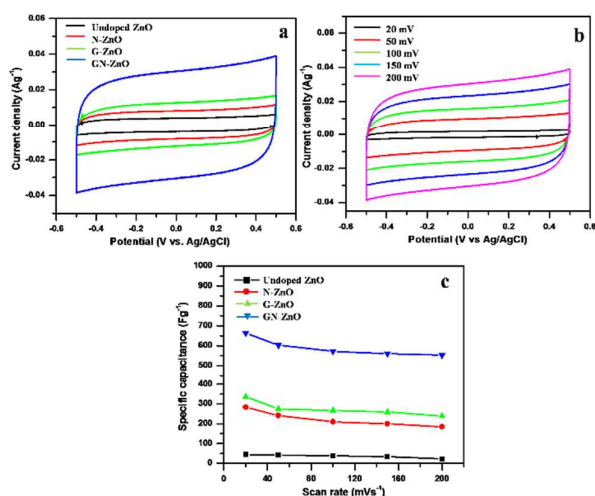


**Fig. 9** Cyclic voltammograms of (a) comparison of cyclic voltammograms of undoped ZnO (Z1), N-ZnO (Z2), ZnO/GR (Z3) and N-ZnO/GR (Z4) at 10 mV s<sup>-1</sup>, (b) N-ZnO/GR (Z4) sample at different scan rates, (c) specific capacitance versus scan rate plots of Z1, Z2, Z3 and Z4 samples.

The curves demonstrate a rectangular and symmetric shape without any distortion even at as high a scan rate as 200 mV s<sup>-1</sup>. This indicates a typical behaviour of supercapacitor having desired fast charging-discharging processes and low contact resistance between electrolyte and electrode.<sup>60</sup> Based on CV curves, the specific capacitance ( $C_s$ , F g<sup>-1</sup>) of the electrode can be calculated according to the following equation:

$$C_s = \frac{\int I dV}{\nu m V} \quad (5)$$

Where  $I$  is the response current (A),  $V$  is the potential (V),  $\nu$  is the potential scan rate (V s<sup>-1</sup>) and  $m$  is the mass of electrode (g). The specific capacitance of samples Z1, Z2, Z3, Z4 are observed to be 22, 185, 239 and 553 F g<sup>-1</sup> respectively, suggesting good electrochemical performance of N-ZnO/GR as an energy storage material. Fig. 9b shows the CV curves for the N-ZnO/GR electrode (in Na<sub>2</sub>SO<sub>4</sub> electrolyte) at different scan rates from 20 to 200 mV s<sup>-1</sup>. At potential scan rates of 20–200 mV s<sup>-1</sup>, the specific capacitances for Z1, Z2, Z3 and Z4 samples are found to be 44–22, 282–185, 336–239 and 663–553 F g<sup>-1</sup> respectively. The CV data show that there is a continuous decrease in the specific capacitance with an increase in the potential scan rate (Fig. 9c), which can be attributed to insufficient time available for ion diffusion and adsorption inside the voids within a sample material.<sup>61</sup> Moreover, the  $C_s$  of the N-ZnO/GR electrode was much higher than that of undoped ZnO, N-ZnO and ZnO/GR electrodes for all the tested scan rates.

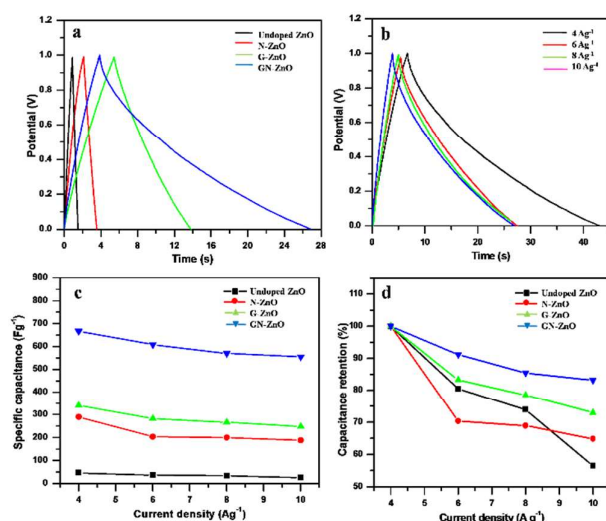


**Fig. 10** Charge–discharge curves of (a) comparison of the charge–discharge profiles of the samples at current density of  $10 \text{ A g}^{-1}$ , (b) N-ZnO/GR sample at different current densities, (c) current density dependent specific capacitance plots of the samples, (d) the plots of capacitance retention versus applied current density of all samples.

Fig. 10a presents the galvanostatic charge–discharge curves of the Z1, Z2, Z3 and Z4 samples measured at current densities of  $10 \text{ A g}^{-1}$ . From the charge–discharge curves tested in the potential range of 0 to 1.0 V, in  $\text{Na}_2\text{SO}_4$  electrolyte, the electrode exhibits nonlinear charge–discharge behaviour. All curves are symmetrical and no obvious voltage drop is observed, which means that the electrodes have low internal resistance due to the well-formed electrode/electrolyte interface. It is to be noted that the discharging time of the N-ZnO/GR sample is higher than that of other three samples, namely, ZnO, N-ZnO and ZnO/GR under identical current density conditions, which indicates a higher electrical capacity for samples.

To accurately determine the electrochemical behaviour of the novel electrodes, the galvanostatic charge–discharge performance of all the samples (Z1–Z4) as electrodes was tested at varying current densities. The average specific capacitance of all the electrodes is calculated as:

$$Cs = \frac{I\Delta t}{m\Delta V} \quad (6)$$

Where  $I$  is constant charge–discharge current (A),  $\Delta t$  is the discharge time (s),  $\Delta V$  is the potential difference (V) during the discharge process, and  $m$  is the total active mass of the electrode (g). The specific capacitances of Z1, Z2, Z3 and Z4 electrodes are established to be 26, 188, 248 and  $555 \text{ F g}^{-1}$  respectively at the current density

of  $10 \text{ A g}^{-1}$ . A comparative discharge profile of N-ZnO/GR sample measured at current densities of 4, 6, 8 and  $10 \text{ A g}^{-1}$ , respectively which is shown in Fig. 10b. It can be seen that at current densities of 4, 6, 8 and  $10 \text{ A g}^{-1}$  the average specific capacitances of N-ZnO/GR are observed to be 667, 608, 570 and  $555 \text{ F g}^{-1}$ , respectively.

The enhanced electrochemical performance of the N-ZnO/GR nanocomposite can be attributed to its hybrid structure. The graphene component of hybrid electrode provides better electronic conductivity and an excellent interfacial contact between N-ZnO and electrolyte, which results in the fast transportation of electrons throughout the entire electrolytic cell.<sup>62</sup> Moreover, it is evident that on doping N in ZnO matrix, the resulting material's (N-ZnO) size is reduced to nanometer scale, which leads great enhancement in the surface area and electro active sites. During the electrochemical process, increased surface area and electroactive sites effectively reduce the diffusion length of the  $\text{Na}^+$  ions in the electrode matrix.<sup>63</sup> Fig. 10c shows a continuous decrease in the specific capacitances for all the samples with increasing current density. Further, from the current density versus capacitance retention plots of the samples as shown in Fig. 10d, it can be ascertained that N-ZnO/GR (Z4) retains  $\sim 83.21\%$  of specific capacitance as against  $\sim 56.52$ ,  $64.83$  and  $72.94\%$  specific capacitance retention by Z1, Z2 and Z3 at  $10 \text{ A g}^{-1}$  respectively. Thus, the data suggests excellent electrochemical performance of N-ZnO/GR as compared to other samples.

**Table 1:** Summary of graphene content, surface area, hydrogen evolution and specific capacitance of synthesized samples

Sample code	Graphene content (%)	$S_{\text{BET}} (\text{m}^2 \text{g}^{-1})$	$\text{H}_2$ ( $\mu\text{mole h}^{-1}$ )	$C_s$ at $10 \text{ A g}^{-1}$
Z1	-	26.56	1874	26
Z2	-	45.26	3957	188
Z3	0.3	40.14	2434	248
Z4	0.3	81.90	5072	555
Z5	0.6	78.39	4784	-
Z6	0.8	75.19	4267	-

Undoped ZnO (Z1) treated at  $800^\circ\text{C}$  for 3h, N-ZnO treated at  $300^\circ\text{C}$  for 3h (Z2), ZnO/GR nanocomposite with 0.3% loading which treated at  $300^\circ\text{C}$  for 3h (Z3) and N-ZnO/GR nanocomposites treated at  $300^\circ\text{C}$  for 3h with different GO loading 0.3% (Z4), 0.6% (Z5), 0.8% (Z6).

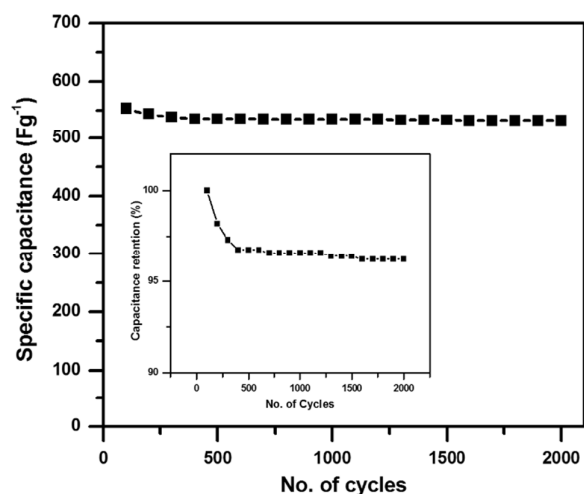


**Fig. 11** Stability of capacitance of N-ZnO/GR (Z4) sample at a current density of  $10 \text{ A g}^{-1}$  in  $1 \text{ M Na}_2\text{SO}_4$  aqueous solution as a function of number of cycles. Inset shows % variation of the specific capacitance of the N-ZnO/GR (Z4) electrode

The long cycle life of the supercapacitors is an important parameter for their practical application. The cycle stability of the N-ZnO/GR hybrid electrode was further evaluated by repeating the CV measurements between 0 and 1.0 V at a scan rate of  $10 \text{ A g}^{-1}$  for 2,000 cycles. (Fig. 11) The capacitance of N-ZnO/GR electrode retained 96.20% of its initial capacitance after 2,000 cycles (inset Fig. 11), which demonstrates excellent electrochemical stability. From these results, we concluded that the N-ZnO/GR electrode material showed a higher specific capacitance, significantly improved energy density, and excellent cycling performance.

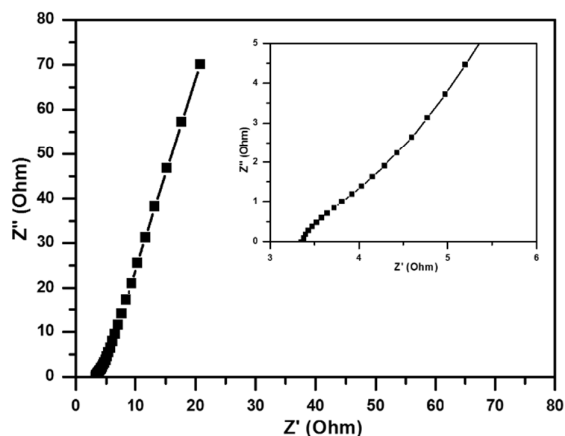


**Fig. 12** Nyquist plot for N-ZnO/GR (Z4) electrode.

The electrochemical performance of N-ZnO/GR (Z4) electrode is also investigated by electrochemical impedance spectroscopy (EIS) (Fig. 12). The nyquist plot of N-ZnO/GR (Z4) electrode exhibits a

small semicircle over the high frequency region (inset of Fig. 12) and straight line in the low frequency region. The  $R_{ct}$  can be directly measured from the Nyquist plot as the semi-circular arc diameter. The  $R_{ct}$  for the N-ZnO/GR (Z4) electrode is  $\sim 4.3 \Omega$ . The low value of  $R_{ct}$  can be rationalized as due to the presence of GR in the composite which will favour the charge transfer across electrode-electrolyte interface, a characteristic behaviour of supercapacitor. The straight line in the low frequency region is called the Warburg resistance ( $R_w$ ). The straight line indicates the pure capacitive behaviour and low resistance for the diffusion resistance of ions in the structure of the electrodes.<sup>64, 65</sup>

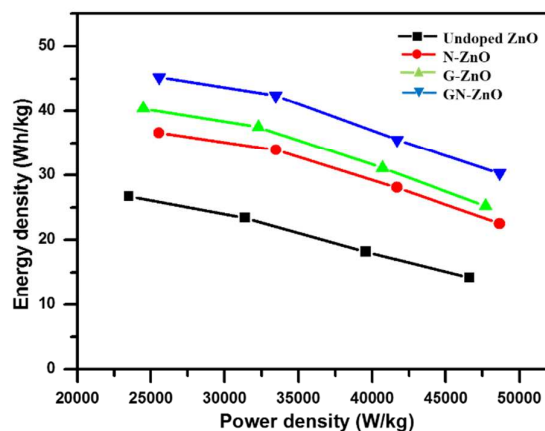


**Fig. 13** Ragone plot of the N-ZnO/GR (Z4) sample.

Fig. 13 shows the Ragone plot which represents the energy density vs power density of the undoped ZnO (Z1), N-ZnO (Z2), ZnO/GR (Z3) and N-ZnO/GR (Z4).

The most critical aspects in the development of supercapacitors is to optimize the energy densities without deteriorating their high power capability as these two parameters determine the ultimate performance of the supercapacitors. According to the Ragone plot of the N-ZnO/GR (Z4) electrode we achieved both high energy density ( $\sim 30 \text{ Wh kg}^{-1}$ ) and high power density ( $\sim 48 \text{ kW kg}^{-1}$ ) simultaneously.

The better electrochemical performance of the as prepared N-ZnO/GR electrode can be attributed to the following aspects:

- 1) Graphene sheets in the composite structure can act as a conducting agent, which greatly improves the electrical conductivity of the composite structure.
- 2) The small size of the N-ZnO nanoparticles were dispersed on the graphene sheets can effectively prevent the agglomeration of ZnO particles, resulting in an improved electrochemical capacitance.

3) Graphene with a large surface area in the composite structure not only provided higher capacitance for energy storage but also helps in fast electron transfer throughout the entire electrode matrix and consequently improves the electrochemical performance.

4) N-ZnO prevents stacking of graphene which improves the electrochemical performance.

Moreover, the nanoparticles of N-ZnO facilitate faster charge-discharge rates because the faradic reaction replaced the diffusion-controlled  $\text{Na}^+$  ion intercalation process which usually occurs at the N-ZnO surface.<sup>66</sup> Therefore, the supercapacitive performance of N-ZnO/GR composite based supercapacitor is significantly improved.

Overall, the result shows that so far unattempted N-ZnO/GR nanocomposite is an excellent stable photocatalyst for hydrogen evolution under solar light. More significantly, its excellent supercapacitive performance shows its potential in energy storage devices.

#### 4. Conclusion

Novel nanocomposite photocatalysts are prepared by decorating N-ZnO nanoparticles on graphene sheets by a facile in-situ wet chemical method. The N-ZnO nanoparticles with a uniform size were decorated onto the graphene sheet. N-ZnO/GR nanocomposite is used for efficient solar hydrogen production from industrial by-product, source of air-pollution, copiously available  $\text{H}_2\text{S}$ . Also, the developed composite has an added feature that it shows the characteristics which suggests its application for supercapacitor which was hitherto un-noticed. The prepared N-ZnO/GR sample showed excellent photocatalytic activity for the hydrogen production ( $\sim 5072 \mu\text{moleh}^{-1}$ ) under solar light. The excellent photocatalytic activity is mainly because of the nitrogen doping, higher surface area, suitable band gap and graphene content. In addition, for supercapacitor, N-ZnO/GR offers many advantages in performance such as high specific capacitance ( $555 \text{ F g}^{-1}$  at  $10 \text{ A g}^{-1}$ ), good charge-discharge stability, long time cycling life. The N-ZnO/GR (Z4) is observed to be a promising electrode material for supercapacitors with high energy and power density. The low price, abundant resources and environmental friendliness of N-ZnO may render their nanocomposites a promising candidate for enhanced photocatalytic and supercapacitive performance.

#### Acknowledgements

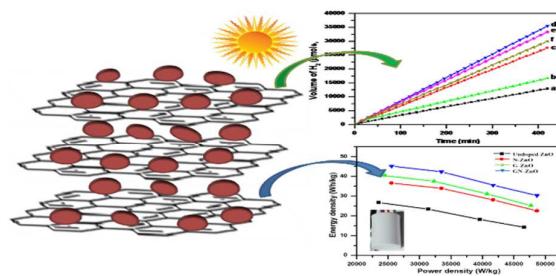
The authors would like to thank C-MET for providing research facilities and Department of Electronics and Information Technology (DeitY), Delhi for their support. Ashwini P. Bhirud would like to thank Council of Scientific and Industrial Research (CSIR) for financial support [9/882(0005) 2K12-EMR-I]. Bharat Kale and Chen-Jin Park is also thankful for the support by MSIP (ministry of science, ICT and future planning), Korea through Brain Pool Program. The authors would also like to thank Dr C. V. Rode, Dr K. R. Patil, NCL and Mr. Sagar Patil, Pune for BET, XPS and electrochemical analysis, respectively. The authors would also like to thank Mr. J. D. Ambekar, C-MET, Pune for FESEM analysis. The authors are very grateful and also wish to express their gratitude to the nanocrystalline materials group C-MET, Pune for their support.

#### Notes and references

- 1 A. Geim and K. Novoselov, *Nat. Mater.*, 2007, **6**, 183-191.
- 2 K. Novoselov, A. Geim, S. Morozov, D. Jiang, Y. Zhang, S. Dubonos, I. Grigorieva and A. Firsov, *Science*, 2004, **306**, 666-669.
- 3 M. Allen, V. Tung and R. B. Kaner, *Chem. Rev.*, 2010, **110**, 132-145.
- 4 Y. Sun, Q. Wu and G. Q. Shi, *Energy Environ. Sci.*, 2011, **4**, 1113-1132.
- 5 Y. Liu, Y. Jiao, Z. Zhang, F. Qu, A. Umar and X. Wu, *ACS Appl. Mater. Interfaces*, 2014, **6**, 2174-2184.
- 6 K. Zhang, L. Zhang, X. Zhao and J. Wu, *Chem. Mater.*, 2010, **22**, 1392-1401.
- 7 C. Xu, B. Xu, Y. Gu, Z. Xiong, J. Sun and X. Zhao, *Energy Environ. Sci.*, 2013, **6**, 1388-1414.
- 8 G. Williams, B. Seger and P. Kamat, *ACS Nano*, 2008, **2**, 1487-1491.
- 9 (a) M. Barbeni, E. Pelizzetti, E. Borgarello, N. Serpone, M. Gratzel and L. Balducci, *Int. J. Hydrogen Energy*, 1985, **10**, 249-253; (b) N. Buhler, K. Meier and J. P. Reber, *J. Phys. Chem.*, 1984, **88**, 3261-3268.
- 10 A. Umar, Y. B. Hahn, *American Scientific Publishers: Los Angeles, CA*, 2010, **5**.
- 11 (a) M. Hoffmann, S. Martin, W. Choi and D. Bahnemann, *Chem. Rev.*, 1995, **95**, 69-96; (b) P. Periyat, S. Pillai, D. McCormack, J. Colreavy and S. Hinder, *J. Phys. Chem. C*, 2008, **112**, 7644-7652; (c) P. Kamat, *J. Phys. Chem. C*, 2007, **111**, 2834-2860; (d) Z. Li, Z.

- Zhou, G. Yun, K. Shi, X. Lv and B. Yang, *Nanoscale Research Letters*, 2013, **8**, 473-481.
- 12 C. Burda, Y. Lou, X. Chen, A. Samia, J. Stout and J. Gole, *Nano Letters*, 2003, **3**, 1049-1051.
- 13 (a) D. Tafen, J. Wang, N. Wu and J. Lewis, *Appl. Phys. Lett.*, 2009, **94**, 093101-093103; (b) H. Irie, Y. Watanabe and K. Hashimoto, *J. Phys. Chem. B*, 2003, **107**, 5483-5486; (c) N. Serpone, *J. Phys. Chem. B*, 2006, **110**, 24287-24293; (d) J. Wang, D. Tafen, J. Lewis, Z. Hong, A. Manivannan, M. Zhi, M. Li and N. Wu, *J. Am. Chem. Soc.*, 2009, **131**, 12290-12297.
- 14 (a) M. Hernandez-Alonso, F. Fresno, S. Suarez and J. Coronado, *Energy Environ. Sci.*, 2009, **2**, 1231-1257; (b) L. Zhang, H. Fu and Y. Zhu, *Adv. Funct. Mater.*, 2008, **18**, 2180-2189.
- 15 (a) J. Yang and S. Gunasekaran, *Carbon*, 2013, **51**, 36-44; (b) L. Zhu, S. Zhang, Y. Cui, H. Song and X. Chen, *Electrochim. Acta*, 2013, **89**, 18-23; (c) Y. Lei, J. Li, Y. Wang, L. Gu, Y. Chang, H. Yuan and D. Xiao, *ACS Appl. Mater. Interfaces*, 2014, **6**, 1773-1780; (d) X. Bin, D. Hui, C. Mo, C. Gaoping and Y. Yusheng, *J. Mater. Chem. A*, 2013, **1**, 4565-4570.
- 16 (a) P. Simon and Y. Gogotsi, *Nat. Mater.*, 2008, **7**, 845-854; (b) G. Xiong, K. Hembram, R. Reifemberger and T. Fisher, *J. Power Sources*, 2013, **227**, 254-259; (c) J. Miller and P. Simon, *Science*, 2008, **321**, 651-652.
- 17 (a) L. Zhang, R. Zhou and X. Zhao, *J. Mater. Chem.*, 2010, **20**, 5983-5992; (b) L. Zhang and X. Zhao, *Chem. Soc. Rev.*, 2009, **38**, 2520-2531.
- 18 H. Long and L. Xianglong, *Adv. Mater.*, 2013, **25**, 3899-3904.
- 19 L. Tingting, Y. Guangwen, W. Jing, Z. Yuanyuan and H. Heyou, *J. Solid State Electrochem.*, 2013, **17**, 2651-2660.
- 20A. Bhirud, S. Sathaye, R. Waichal, J. Ambekar, C. Park and B. Kale, *Nanoscale*, 2015, **7**, 5023-5034.
- 21 (a) M. Yang, N. Zhang, M. Pagliaro and Y. Xu, *Chem. Soc. Rev.*, 2014, **43**, 8240-8254; (b) N. Zhang, Y. Zhang and Y. Xu, *Nanoscale*, 2012, **4**, 5792-5813; (c) M. Yang and Y. Xu, *Phys. Chem. Chem. Phys.*, 2013, **15**, 19102-19118; (d) N. Zhang, M. Yang, Z. Tang and Y. Xu, *ACS Nano*, 2014, **8**, 623-633; (e) Y. Zhang, Z. Tang, X. Fu, and Y. Xu, *ACS Nano*, 2010, **4**, 7303-7314; (f) Y. Zhang, Z. Tang, X. Fu, and Y. Xu, *ACS Nano*, 2011, **5**, 7426-7435; (g) C. Guan, J. Liu, Y. Wang, L. Mao, Z. Fan, Z. Shen, H. Zhang and J. Wang, *ACS Nano*, 2015, **9**, 5198-5207; (h) U. Shao, Maher F. Kady, L. Wang, Q. Zhang, Y. Li, H. Wang, M. Mousavi and R. Kaner, *Chem. Soc. Rev.*, 2015, **44**, 3639-3665.
- 22X. Dong, Y. Cao, J. Wang, M. Chan-Park, L. Wang, W. Huang and P. Chen, *RSC Adv.*, 2012, **2**, 4364-4369.
- 23Y. Zhang, Z. Chen, S. Liu and Y. Xu, *Applied Catalysis B: Environmental*, 2013, **140-141**, 598-607.
- 24A. Prakash and D. Bahadur, *ACS Appl. Mater. Interfaces*, 2014, **6**, 1394-1405.
- 25 Y. Feng, N. Feng, Y. Wei and G. Zhang, *RSC Adv.*, 2014, **4**, 7933-7943.
- 26 (a) B. Weng, M. Yang, N. Zhang and Y. Xu, *J. Mater. Chem. A*, 2014, **2**, 9380-9389; (b) Z. Chen, N. Zhang and Y. Xu, *CrystEngComm*, 2013, **15**, 3022-3030; (c) X. Pan, M. Yang and Y. Xu, *Phys. Chem. Chem. Phys.*, 2014, **16**, 5589-5599.
- 27 A. Bhirud, S. Sathaye, R. Waichal, L. Nikam and B. Kale, *Green Chem.*, 2012, **14**, 2790-2798.
- 28W. Hummers and R. Offeman, *J. Am. Chem. Soc.*, 1958, **80**, 1339.
- 29 (a) F. Xiao, F. Wang, X. Fu and Y. Zheng, *J. Mater. Chem.*, 2012, **22**, 2868-2877; (b) X. Liu, L. Pan, Q. Zhao, T. Lv, G. Zhu, T. Chen, T. Lu, Z. Sun and C. Sun, *Chem. Eng. J.*, 2012, **183**, 238-243; (c) F. Xiao, *ACS Appl. Mater. Interfaces*, 2012, **4**, 7055-7063.
- 30H. Zhang, X. Lv, Y. Li, Y. Wang and J. Li, *ACS Nano*, 2010, **4**, 380-386.
- 31Z. Jiang, L. Kong, F. Sh. Alenazey, Y. Qian, L. France, T. Xiao and P. Edwards, *Nanoscale*, 2013, **5**, 5396-5402.
- 32 (a) Q. Xiang, J. Yu and M. Jaroniec, *J. Phys. Chem. C*, 2011, **115**, 7355-7363; (b) Q. Xiang, J. Yu and M. Jaroniec, *Nanoscale*, 2011, **3**, 3670-3678.
- 33 K. Saito, Y. Hosokai, K. Nagayama, K. Ishida, K. Takahashi, M. Konagai and B. Zhang, *J. Cryst. Growth*, 2004, **272**, 805-809.
- 34 X. Zhu, H. Wu, D. Qiu, Z. Yuan, G. Jin, J. Kong and W. Shen, *Opt. Commun.*, 2010, **283**, 2695-2699.
- 35 (a) B. Sieber, H. Liu, G. Piret, J. Laureyns, P. Roussel, B. Gelloz, S. Szunerits and R. Boukherroub, *J. Phys. Chem. C*, 2009, **113**, 13643-13650; (b) G. Du, Y. Ma, Y. Zhang and T. Yang, *Appl. Phys. Lett.*, 2005, **87**, 213103-3.
- 36Q. Zhang, C. Tian, A. Wu, T. Tan, L. Sun, L. Wang and H. Fu, *J. Mater. Chem.*, 2012, **22**, 11778-11784.
- 37 (a) O. Akhavan, *Carbon*, 2015, **81**, 158-166; (b) I. Calizo, A. Balandin, W. Bao, F. Miao and C. Lau, *Nano Lett.*, 2007, **7**, 2645-2649; (c) K. Kudin, B. Ozbas, H. Schniepp, R. Prud'homme, I. Aksay and R. Car, *Nano Lett.*, 2008, **8**, 36-41; (d) K. Kim, Y. Zhao, H. Jang, S. Lee, J. Kim, K. Kim, J. Ahn, P. Kim, J. Choi and B. Hong, *Nature*, 2009, **457**, 706-710; (e) A. Ferrari, J. Meyer, V. Scardaci,

- C. Casiraghi, M. Lazzeri, F. Mauri, S. Piscanec, D. Jiang, K. Novoselov, S. Roth and A. Geim, *Phys. Rev. Lett.*, 2006, **97**, 187401-187404.
- 38(a) S. Liu, C. Liu, W. Wang, B. Cheng and J. Yu, *Nanoscale*, 2012, **4**, 3193-3200; (b) W. Wang, J. Yu, Q. Xiang and B. Cheng, *Applied Catalysis B: Environmental*, 2012, **119-120**, 109-116; (c) N. Farhangi, R. Chowdhury, Y. Gonzalez, M. Ray and P. Charpentier, *Applied Catalysis B: Environmental*, 2011, **110**, 25-32.
- 39 O. Akhavan, *ACS Nano*, 2010, **4**, 4174-4180.
- 40 Q. Zhang, C. Tian, A. Wu, T. Tan, L. Sun, L. Wang and H. Fu, *J. Mater. Chem.*, 2012, **22**, 11778-11784.
- 41 O. Akhavan, *Acs Nano*, 2010, **4**, 4174-4180.
- 42 M. Samadi, H. Shivaee, M. Zanetti, A. Pourjavadi and A. Moshfegh, *J. Mol. Catal. A-Chem.*, 2012, **359**, 42-48.
- 43 S. Anandana, A. Vinu, K. Lovely, N. Gokulakrishnan, P. Srinivasu, T. Mori, V. Murugesan, V. Sivamurugan and K. Ariga, *J. Mol. Catal. A: Chem.*, 2007, **266**, 149-157.
- 44 S. Chen, S. Zhang, W. Liu and W. Zhao, *J. Hazard. Mater.*, 2008, **155**, 320-326.
- 45 S. Chen and L. Chen, *Mater. Chem. Phys.*, 2006, **98**, 116-120.
- 46 (a) H. Wang, H. Ho, K. Lo and K. Cheah, *J. Phys. D: Appl. Phys.*, 2007, **40**, 4682-4685; (b) C. Perkins, S. Lee, X. Li, S. Asher and T. Coutts, *J. Appl. Phys.*, 2005, **97**, 034907-7.
- 47 Q. Li, B. Guo, J. Yu, J. Ran, B. Zhang, H. Yan, and J. Gong, *J. Am. Chem. Soc.*, 2011, **133**, 10878-10884.
- 48 Q. Li, B. Guo, J. Yu, J. Ran, B. Zhang, H. Yan and J. Gong, *J. Am. Chem. Soc.*, 2011, **133**, 10878-10884.
- 49 (a) J. Ding, M. Wang, J. Deng, W. Gao, Z. Yang, C. Ran and X. Zhang, *J. Alloys Compd.*, 2014, **582**, 29-32; (b) W. Wang, D. Wang, W. Qu, L. Lu and A. Xu, *J. Phys. Chem. C*, 2012, **116**, 19893-19901.
- 50 Y. Tang, C. Lee, J. Xu, Z. Liu, Z. Chen, Z. He, Y. Cao, G. Yuan, H. Song, L. Chen, L. Luo, H. Cheng, W. Zhang, I. Bello and S. Lee, *ACS Nano*, 2010, **4**, 3482-3488.
- 51 Z. Lei, L. Lu and X. Zhao, *Energy Environ. Sci.*, 2012, **5**, 6391-6399.
- 52 G. Williams, B. Seger and P. Kamat, *ACS Nano*, 2008, **2**, 1487-1491.
- 53 J. Yu, H. Yu, B. Cheng, M. Zhou and X. Zhao, *J. Mol. Catal. A*, 2006, **253**, 112-118.
- 54 J. Yu, T. Ma and S. Liu, *Phys. Chem. Chem. Phys.*, 2011, **13**, 3491-3501.
- 55 N. Chaudhari, S. Warule, S. Dhanmane, M. Kulkarni, M. Valant and B. Kale, *Nanoscale*, 2013, **5**, 9383-9390.
- 56 (a) B. Kale, J. Baeg, S. Lee, H. Chang, S. Moon and C. Lee, *Adv. Funct. Mater.*, 2006, **16**, 1349-1354; (b) A. Bhirud, N. Chaudhari, L. Nikam, R. Sonawane, K. Patil, B. Ook and B. Kale, *Int. J. Hydrogen Energy*, 2011, **36**, 11628-11639; (c) S. Apte, S. Garje, G. Mane, A. Vinu, S. Naik, D. Amalnerkar and B. Kale, *Small*, 2011, **7**, 957-964; (d) S. Apte, S. Garaje, S. Naik, R. Waichal, J. Baeg, B. Kale, *Nanoscale*, 2014, **6**, 908-915.
- 57 N. Yang, J. Zhai, D. Wang, Y. Chen and L. Jiang, *ACS Nano*, 2010, **4**, 887-894.
- 58 H. Nian, S. Hahn, K. Koo, E. Shin and E. Kim, *Materials Letters*, 2009, **63**, 2246-2248.
- 59 T. Lv, L. Pan, X. Liu and Z. Sun, *Catal. Sci. Technol.*, 2012, **2**, 2297-2301.
- 60 (a) Y. Sun, Q. Wu and G. Shi, *Phys. Chem. Chem. Phys.*, 2011, **13**, 17249-17254; (b) T. Kim, H. Lee, M. Stoller, D. Dreyer, C. Bielawski, R. Ruoff and K. Suh, *ACS Nano*, 2011, **5**, 436-442; (c) Y. Zhu, S. Murali, M. Stoller, K. Ganesh, W. Cai, P. Ferreira, A. Pirkle, R. Wallace, K. Cychosz, M. Thommes, D. Su, E. Stach and R. Ruoff, *Science*, 2011, **332**, 1537-1541; (d) S. Chen, J. Zhu, X. Wu and Q. Han, *ACS Nano*, 2010, **4**, 2822-2830.
- 61 D. Dubal and R. Holze, *Energy*, 2013, **51**, 407-412.
- 62 Y. Kim, J. Lee and G. Yi, *Appl Phys Lett*, 2009, **95**, 213101-3.
- 63 (a) S. Kim, M. Parvez, M. Chhowalla, *Chem Phys Lett*, 2009, **483**, 124-127; (b) J. Chen, C. Li, G. Eda, Y. Zhang, W. Lei, M. Chhowalla, W. Milne and W. Deng, *Chem Commun*, 2011, **47**, 6084-6086.
- 64 E. Frackowiak and F. Beguin, *Carbon*, 2001, **39**, 937-950.
- 65 S. Shi, X. Zhuang, B. Cheng and X. Wang, *J. Mater. Chem. A*, 2013, **1**, 13779-13788.
- 66 M. Jayalakshmi, M. Palaniappa, K. Balasubramanian, *Int. J. Electrochem. Sci.*, 2008, **3**, 96-103.



N-ZnO/GR nanocomposite is synthesized by in-situ wet chemical method which shows superior photocatalytic H<sub>2</sub> production and high supercapacitive performance.